
Unveiling Transformer Perception by Exploring Input Manifolds

Alessandro Benfenati

Department of Environmental Science and Policy
 Università degli Studi di Milano
 Milano, Italy
 alessandro.benfenati@unimi.it

Alfio Ferrara

Department of Computer Science
 Università degli Studi di Milano
 Milano, Italy
 alfio.ferrara@unimi.it

Alessio Marta

Dipartimento di Scienze del Sistema Nervoso e del Comportamento
 Università di Pavia
 Pavia, Italy
 alessio.marta@unipv.it

Davide Riva

Department of Control and Computer Engineering
 Politecnico di Torino
 Torino, Italy
 davide.riva@polito.it

Elisabetta Rocchetti

Department of Computer Science
 Università degli Studi di Milano
 Milano, Italy
 elisabetta.rocchetti@unimi.it

Abstract

This paper introduces a general method for the exploration of equivalence classes in the input space of Transformer models. The proposed approach is based on sound mathematical theory which describes the internal layers of a Transformer architecture as sequential deformations of the input manifold. Using eigendecomposition of the pullback of the distance metric defined on the output space through the Jacobian of the model, we are able to reconstruct equivalence classes in the input space and navigate across them. We illustrate how this method can be used as a powerful tool for investigating how a Transformer sees the input space, facilitating local and task-agnostic explainability in Computer Vision and Natural Language Processing tasks.

1 Introduction

In this paper, we propose a method for exploring the input space of Transformer models by identifying equivalence classes with respect to their predictions. We define an *equivalence class* of a Transformer model as the set of vectors in the embedding space whose outcomes under the Transformer process are the same. The study of the input manifold on which the inverse image of models lies provides insights for both explainability and sensitivity analyses. Existing methods aiming at the exploration of the input space of Deep Neural Networks and Transformers either rely on perturbations of input data using heuristic or gradient-based criteria [16, 22, 17, 14], or they analyze specific properties of the embedding space [5].

Our approach is based on sound mathematical theory which describes the internal layers of a Transformer architecture as sequential deformations of the input manifold. Using eigendecomposition of the pullback of the distance metric defined on the output space through the Jacobian of the model,

we are able to reconstruct equivalence classes in the input space and navigate across them. In the XAI scenario, our framework can facilitate local and task-agnostic explainability methods applicable to Computer Vision (CV) and Natural Language Processing (NLP) tasks, among others.

In Section 2, we summarise the preliminaries of the mathematical foundations of our approach. In Section 3, we present our method for the exploration of equivalence classes in the input of the Transformer models. In Section 4, we perform a preliminary investigation of some applicability options of our method on textual and visual data. In Section 5, we discuss the relevant literature about embedding space exploration and feature importance. Finally, in Section 6, we give our concluding remarks¹.

2 Preliminaries

In this Section, we provide the theoretical foundation of the proposed approach, namely the Geometric Deep Learning framework based on Riemannian Geometry [2].

A neural network is considered as a sequence of maps, the layers of the network, between manifolds, and the latter are the spaces where the input and the outputs of the layers belong to.

Definition 1 (Neural Network). *A neural network is a sequence of \mathcal{C}^1 maps Λ_i between manifolds of the form:*

$$M_0 \xrightarrow{\Lambda_1} M_1 \xrightarrow{\Lambda_2} M_2 \xrightarrow{\Lambda_4} \dots \xrightarrow{\Lambda_{n-1}} M_{n-1} \xrightarrow{\Lambda_n} M_n \quad (1)$$

We call M_0 the input manifold and M_n the output manifold. All the other manifolds of the sequence are called representation manifolds. The maps Λ_i are the layers of the neural network. We denote with $\mathcal{N}_{(i)} = \Lambda_n \circ \dots \circ \Lambda_i : M_i \rightarrow M_n$ the mapping from the i -th representation layer to the output layer.

As an example, consider a shallow network with just one layer, the composition of a linear operator $A \cdot + b$ with a sigmoid function σ , where $A \in \mathbb{R}^{m \times n}$ and $b \in \mathbb{R}^m$: then, the input manifold M_0 and the output manifold M_1 shall be \mathbb{R}^n and \mathbb{R}^m , respectively, and the map $\Lambda_1(\cdot) = \sigma(A \cdot + b)$. We generalize this observation into the following definition.

Definition 2 (Smooth layer). *A map $\Lambda_i : M_{i-1} \rightarrow M_i$ is called a smooth layer if it is the restriction to M_{i-1} of a function $\bar{\Lambda}^{(i)}(x) : \mathbb{R}^{d_{i-1}} \rightarrow \mathbb{R}^{d_i}$ of the form*

$$\bar{\Lambda}^{(i)}(x) = F_\alpha^{(i)} \left(\sum_\beta A_{\alpha\beta}^{(i)} x_\beta + b_\alpha^{(i)} \right) \quad (2)$$

for $i = 1, \dots, n$, $x \in \mathbb{R}^{d_i}$, $b^{(i)} \in \mathbb{R}^{d_i}$ and $A^{(i)} \in \mathbb{R}^{d_i \times d_{i-1}}$, with $F^{(i)} : \mathbb{R}^{d_i} \rightarrow \mathbb{R}^{d_i}$ a diffeomorphism.

Remark 1. *Transformers implicitly apply for this framework, since their modules are smooth functions, such as fully connected layers, GeLU and sigmoid activations.*

Our aim is to transport the geometric information on the data lying in the output manifold to the input manifold: this allows us to obtain insight on how the network "sees" the input space, how it manipulates it for reaching its final conclusion. For fulfilling this objective, we need several tools from differential geometry. The first key ingredient is the notion of singular Riemannian metric, which has the intuitive meaning of a degenerate scalar product which changes point to point.

Definition 3 (Singular Riemannian metric). *Let $M = \mathbb{R}^n$ or an open subset of \mathbb{R}^n . A singular Riemannian metric g over M is a map $g : M \rightarrow \text{Bil}(\mathbb{R}^n \times \mathbb{R}^n)$ that associates to each point p a positive semidefinite symmetric bilinear form $g_p : \mathbb{R}^n \times \mathbb{R}^n \rightarrow \mathbb{R}$ in a smooth way.*

Without loss of generality, we can assume the following hypotheses on the sequence (1): *i*) The manifolds M_i are open and path-connected sets of dimension $\dim M_i = d_i$. *ii*) The maps Λ_i are \mathcal{C}^1 submersions. *iii*) $\Lambda_i(M_{i-1}) = M_i$ for every $i = 1, \dots, n$. *iv*) The manifold M_n is equipped with the structure of Riemannian manifold, with metric $g^{(n)}$. Definition 3 naturally leads to the definition of the pseudolength and of energy of a curve.

¹The code to reproduce our experiments can be found in the Supplementary Materials.

Definition 4 (Pseudolength and energy of a curve). *Let $\gamma : [a, b] \rightarrow \mathbb{R}^n$ a curve defined on the interval $[a, b] \subset \mathbb{R}$ and $\|v\|_p = \sqrt{g_p(v, v)}$ the pseudo-norm induced by the pseudo-metric g_p at point p . Then the pseudolength of γ and its energy are defined as*

$$Pl(\gamma) = \int_a^b \|\dot{\gamma}(s)\|_{\gamma(s)} ds = \int_a^b \sqrt{g_{\gamma(s)}(\dot{\gamma}(s), \dot{\gamma}(s))} ds, \quad E(\gamma) = \int_a^b \|\dot{\gamma}(s)\|_{\gamma(s)}^2 ds \quad (3)$$

The notion of pseudolength leads naturally to define the distance between two points.

Definition 5 (Pseudodistance). *Let $x, y \in M = \mathbb{R}^n$. The pseudodistance between x and y is then*

$$Pd(x, y) = \inf\{Pl(\gamma) \mid \gamma : [0, 1] \rightarrow M, \gamma \in \mathcal{C}^1([0, 1]), \gamma(0) = x, \gamma(1) = y\}. \quad (4)$$

One can observe that endowing the space \mathbb{R}^n with a singular Riemannian metric leads to have non trivial curves whose length is zero. A straightforward consequence is that there are distinct points whose pseudodistance is therefore zero: a natural equivalence relation arises, *i.e.* $x \sim y \Leftrightarrow Pd(x, y) = 0$, obtaining thus a metric space $(\mathbb{R}^n / \sim, Pd)$.

The second crucial tool is the notion of pullback of a function. Let f be a function from \mathbb{R}^p to \mathbb{R}^q , and fix the coordinate systems $x = (x_1, \dots, x_p)$ and $y = (y_1, \dots, y_q)$ on \mathbb{R}^p and on \mathbb{R}^q , respectively. Moreover, we endow \mathbb{R}^q with the standard Euclidean metric g , whose associated matrix is the identity. The space \mathbb{R}^p can be equipped with the pullback metric f^*g whose representation matrix reads as

$$(f^*g)_{ij} = \sum_{h,k=1}^q \left(\frac{\partial f_h}{\partial x_i} \right) g_{hk} \left(\frac{\partial f_k}{\partial x_j} \right). \quad (5)$$

The sequence (1) shows that a neural network can be considered simply as a function, a composition of maps: hence, taking $f = \Lambda_n \circ \Lambda_{n-1} \circ \dots \circ \Lambda_1$ and supposing that $M_0 = \mathbb{R}^p, M_n = \mathbb{R}^q$, the generalization of (5) applied to (1) provides with the pullback of a generic neural network.

Hereafter, we consider in (1) the case $M_n = \mathbb{R}^q$, equipped with the trivial metric $g^{(n)} = I_q$, *i.e.*, the identity. Each manifold M_i of the sequence (1) is equipped with a Riemannian singular metric, denoted with $g^{(i)}$, obtained via the pullback of $\mathcal{N}_{(i)}$. The pseudolength of a curve γ on the i -th manifold, namely $Pl_i(\gamma)$, is computed via the relative metric $g^{(i)}$ via (3).

2.1 General results

We depict hereafter the theoretical bases of our approach. We denote with \mathcal{N}_i the submap $\Lambda_i \circ \dots \circ \Lambda_n : M_i \rightarrow M_n$, and with $\mathcal{N} \equiv \mathcal{N}_0$ the map describing the action of the complete network. The starting point is to consider the pair (M_i, Pd_i) : this is a pseudometric space, which can be turned into a full-fledged metric space M_i / \sim_i by the metric identification $x \sim_i y \Leftrightarrow Pd_i(x, y) = 0$. The first result states that the length of a curve on the i -th manifold is preserved among the mapping on the subsequent manifolds.

Proposition 1. *Let $\gamma : [0, 1] \rightarrow M_i$ be a piecewise \mathcal{C}^1 curve. Let $k \in \{i, i+1, \dots, n\}$ and consider the curve $\gamma_k = \Lambda_k \circ \dots \circ \Lambda_i \circ \gamma$ on M_k . Then $Pl_i(\gamma) = Pl_k(\gamma_k)$.*

In particular this is true when $k = n$, *i.e.*, the length of a curve is preserved in the last manifold. This result leads naturally to claim that if two points are in the same class of equivalence, then they are mapped into the same point under the action of the neural network.

Proposition 2. *If two points $p, q \in M_i$ are in the same class of equivalence, then $\mathcal{N}_i(p) = \mathcal{N}_i(q)$.*

The next step is to prove that the sets M_i / \sim_i are actually smooth manifolds: to this aim, we introduce another equivalence relation: $x \sim_{\mathcal{N}_i} y$ if and only if there exists a piecewise $\gamma : [0, 1] \rightarrow M_i$ such that $\gamma(0) = x, \gamma(1) = y$ and $\mathcal{N}_i \circ \gamma(s) = \mathcal{N}_i(x) \forall s \in [0, 1]$. The introduction of this equivalence relation allows us to easily state the following proposition.

Proposition 3. *Let $x, y \in M_i$, then $x \sim_i y$ if and only if $x \sim_{\mathcal{N}_i} y$.*

The following corollary contains the natural consequences of the previous result; the second point of the claim below is the counterpart of Proposition 2.

Corollary 1. *Under the hypothesis of Proposition 3, one has that $M_i/\sim_i = M_i/\sim_{N_{i+1}}$. Moreover, if two points $p, q \in M_i$ are connected by a C^1 curve $\gamma : [0, 1] \rightarrow M_i$ satisfying $N_i(p) = N_i \circ \gamma(s)$ for every $s \in [0, 1]$, then they lie in the same class of equivalence.*

Making use of the Godement's criterion, we are now able to prove that the set M_i/\sim_i is a smooth manifold, together with its dimension.

Proposition 4. $\frac{M_i}{\sim_i}$ is a smooth manifold of dimension $\dim(\mathcal{N}(M_0))$.

This last achievement provides practical insights about the projection π_i on the quotient space, that consists the building block of the algorithms used for recovering and exploring the equivalence classes of a neural network.

Proposition 5. $\pi_i : M_i \rightarrow M_i/\sim_i$ is a smooth fiber bundle, with $\text{Ker}(d\pi_i) = \mathcal{V}M_i$, which is therefore an integrable distribution. $\mathcal{V}M_i$ is the vertical bundle of M_i . Every class of equivalence $[p]$ is a path-connected submanifold of M_i and coincide with the fiber of the bundle over the point $p \in M_i$.

3 Methodology

The results depicted in Section 2.1 provide powerful tools for investigating how a neural network sees the input space starting from a point x . In particular we point out the following remarks: i) If two points x, y belonging to the input manifold M_0 are such that $x \sim_0 y$, then $\mathcal{N}(x) = \mathcal{N}(y)$; ii) given a point $p \in M_n$, the counterimage $\mathcal{N}^{-1}(p)$ is a smooth manifold, whose connected components are classes of equivalences in M_0 with respect to \sim_0 . A necessary condition for two points $x, y \in M_0$ to be in the same class of equivalence is that $\mathcal{N}(x) = \mathcal{N}(y)$; iii) any class of equivalence $[x]$, $x \in M_0$, is a maximal integral submanifold of $\mathcal{V}M_0$. The above observations directly provide with a strategy to build up the equivalence class of an input point $x \in M_0$. Proposition 5 tells us that $\mathcal{V}M_0$ is an integrable distribution, with dimension equal to the dimension of the kernel of $g^{(0)}$: we can hence find $\dim(\text{Ker}(g^{(0)}))$ vector fields which are a base for the tangent space of M_0 . This means that we can compute the eigenvalue decomposition of $g_x^{(0)}$ and consider the L linearly independent eigenvectors, namely $\{v_l\}_{l=1, \dots, L}$, associated to the null eigenvalue: these eigenvectors depend *smoothly* on the point, a fact that is not trivial when the matrix associated to the metric depends on several parameters [15]. We can build then all the null curves by randomly selecting one eigenvector $\tilde{v} \in \{v_l\}$ and then reconstruct the curve along the direction \tilde{v} from the starting point x . From a practical point of view, one is led to solve the Cauchy problem, a first order differential equation, with $\dot{\gamma} = \tilde{v}$ and initial condition $\gamma(0) = x$.

3.1 Input Space Exploration

This whole procedure is coded in the Singular Metric Equivalence Class (SiMEC) and the Singular Metric Exploration (SiMExp) algorithms, whose general schemes are depicted in Algorithms 1 and 2. SiMEC reconstructs the class of equivalence of the input via the exploration of the input space by randomly selecting one of the eigenvectors related to the zero eigenvalue. On the opposite, in SiMExp, in order to move from a class of equivalence to another we consider the eigenvectors relative to the nonzero eigenvalues. This requires the slight difference in lines 5 to 7 between Algorithm 1 and Algorithm 2.

Algorithm 1 The Singular Metric Equivalence Class (SiMEC) algorithm.

- 1: Set the network \mathcal{N} ; choose the maximum number of iterations. Choose the input p_0 .
- 2: **for** $k = 0, 1, \dots, K - 1$ **do**
- 3: Compute $g_{\mathcal{N}(p_k)}^n$
- 4: Compute the pullback metric $g_{p_k}^0$
- 5: Diagonalize $g_{p_k}^0$ and find the eigenvectors $\{v_l\}_l$ associated to the zero eigenvalue
- 6: Randomly select $\tilde{v} \in \{v_l\}_l$
- 7: $\delta = 1/\sqrt{\max(\text{eigenvalues of } g_{p_k}^0)}$
- 8: $p_{k+1} \leftarrow p_k + \delta \tilde{v}$
- 9: **end for**
- 10: Optionally: store $\{p_k\}_{k=0, \dots, K}$ for optimizing future computations
- 11: Project p_k to the nearest feasible region

Algorithm 2 The Singular Metric Exploration (SiM-Exp) algorithm.

- 1: Set the network \mathcal{N} ; choose the maximum number of iterations. Choose the input p_0 .
- 2: **for** $k = 0, 1, \dots, K - 1$ **do**
- 3: Compute $g_{\mathcal{N}(p_k)}^n$
- 4: Compute the pullback metric $g_{p_k}^0$
- 5: Diagonalize $g_{p_k}^0$ and find the eigenvectors $\{w_l\}_l$ associated to the non-zero eigenvalue
- 6: Randomly select $\tilde{w} \in \{w_l\}_l$
- 7: $\delta = 2/\sqrt{\max(\text{eigenvalues of } g_{p_k}^0)}$
- 8: $p_{k+1} \leftarrow p_k + \delta \tilde{w}$
- 9: **end for**
- 10: Optionally: store $\{p_k\}_{k=0, \dots, K}$ for optimizing future computations
- 11: Project p_k to the nearest feasible region

There are some remarks to point out. From a numerical point of view, the diagonalization of the pullback may lead to have even negative eigenvalues: hence one may use the notion of energy of a curve, related to the pseudolength. The update rule for the new point (line 8) amounts to solve the differential problem via the Euler method: for a reliable solution, we suggest to choose a small step-length δ . On the other hand, if the value of δ is too small more iterations are needed to move away from the starting point sensibly. Therefore there is a trade-off between the reliability of the solution and the exploration pace. The proof of the well-posedness theorem for Cauchy problems, cf. [18, Theorem 2.1], yields some insights, suggesting to set δ equal to the inverse of the Lipschitz constant of the map \mathcal{N} – which in practice we can estimate with the inverse of the square root of the largest eigenvalue λ_M of the pullback metric $g_{p_k}^0$. This is our default choice for Algorithm 1. We also note that Algorithm 1 is more sensitive to the choice of the parameter δ compared to Algorithm 2. To build points in the same equivalence class Algorithm 1 needs to follow a null curve closely with as little approximations as possible, namely with a small δ . In contrast Algorithm 2, whose goal is to change the equivalence class from one iteration to the next, does not have the same problem and larger δ are allowed. Our default choice is therefore to set $\delta = 2\lambda_M^{-1/2}$ for Algorithm 2. As for the computational complexity of the two algorithms, the most demanding step is the computation of the eigenvalues and eigenvectors, which is $O(n^3)$, with n the dimension of the square matrix $g_{p_k}^0$ [20]. Since all the other operations are either $O(n)$ or $O(n^2)$, we conclude that the complexity of both Algorithms 1 and 2 is $O(n^3)$.

3.2 Interpretability

Algorithms 1 and 2 allow for the exploration of the equivalence classes in the input space of a Transformer model. However, the points explored by these algorithms may not be directly interpretable by a human perspective. For instance, an image or a piece of text may need to be decoded to be “readable” by a human observer. Furthermore, we present an interpretation of the eigenvalues of the pullback metric which allows us to define a feature importance metric. We present two interpretability methods for Transformers based on input space exploration. Both methods are then demonstrated on a Vision Transformer (ViT) trained for digit classification [8], and two BERT models, one trained for hate speech classification and the other trained for MLM [7, 19].

Algorithm 3 Feature Importance Analysis Using Pull-back Metric $g_{x^e}^0$

- 1: **Inputs:**
- 2: Transformer model T with: Tokenizer t_T , Embedding layer e_T , Intermediate layers l_T
- 3: Input data x
- 4: Tokenize input x to obtain tokens $x^t = t_T(x)$
- 5: Compute embeddings $x^e = e_T(x^t)$
- 6: Compute intermediate representations $g_{l_T(x^e)}^n$
- 7: Calculate the pullback metric $g_{x^e}^0$
- 8: Diagonalize $g_{x^e}^0$ to extract eigenvalues
- 9: Identify the maximum eigenvalue for each embedding, indicating its importance
- 10: **Output:** Heatmap of embedding importance based on the eigenvalues

Algorithm 4 Exploration of Embedding Space in Transformers

- 1: **Inputs:**
- 2: Transformer model T with: Tokenizer t_T , Embedding layer e_T , Intermediate layers l_T
- 3: Input data x (image or text)
- 4: Retrieve segments $x^t = t_T(x)$.
- 5: Choose segments $P = \{p | p \in x^t\}$ for updates; keep others unchanged.
- 6: Compute embeddings $x^e = e_T(x^t)$.
- 7: Apply SiMEC or SiMExp on x^e , updating embeddings for segments in P .
- 8: **Outputs:** Modified input embedding, one for each SiMEC/SiMExp iteration.

Feature importance. Consider a Transformer model T whose architecture includes a tokenizer t_T (or patcher for images) that segments the input so that each segment can be converted into a continuous representation by an embedding layer e_T . This results in a matrix of dimensions $n_s \times h$, where n_s represents the number of segments, and h denotes the hidden size of the model’s embeddings. The eigenvalues of the pullback metric can be used to deduce the importance of each embedding and, by extension, the significance of the segments they represent, with respect to the final prediction. The process for determining the importance of textual tokens or image patches is outlined in Algorithm 3. The appearance of the resulting heatmaps varies according to the type of input used. An example of experiments with ViT on the MNIST dataset [12] is shown in Figure 1 that depicts heatmaps for two MNIST instances. Figure 2, on the left, illustrates two experiments using Algorithm 3 on both a

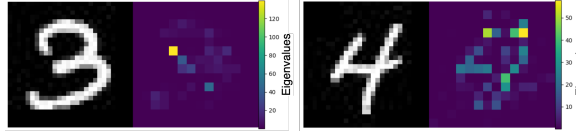


Figure 1: Example output from Algorithm 3 applied to digit classification. These two instances are predicted as 3 (left) and 4 (right). The brightness of the color indicates the eigenvalue’s magnitude. The brighter the color, the more sensitive the patch. This indicates that changes in the values of these sensitive patches are likely to have a greater impact on the prediction probabilities. Each patch in the heatmap corresponds to a 2×2 square pixel.

BERT model for hate speech detection and a BERT model for MLM.

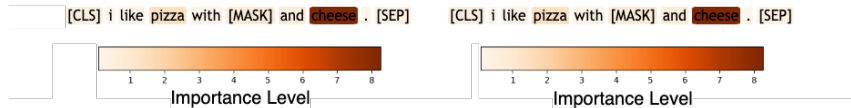


Figure 2: Example outputs from Algorithm 3. The darker the color, the higher the token’s eigenvalue. Left: The sentence analysed is classified as “offensive” by the BERT for hate speech detection, with significant contributions from tokens [CLS], politicians, corrupt, and #eit (part of the word *deceitful*). Right: Example instance processed by a BERT model for masked language modeling. [MASK] is predicted as “ham”, with the most influential tokens being pizza and cheese.

Interpretation of input space exploration. Using SiMEC and SiMExp to explore the embedding space reveals how Transformer models perceive equivalence among different data points. Specifically, these methodologies facilitate the sequential acquisition of embedding matrices $p_0 \dots p_K$ at each iteration, as detailed in Algorithms 1 and 2. Algorithm 4 implements a practical application of the SiMEC/SiMExp approach with Transformer models. A key feature of this method is its ability

to selectively update specific tokens (for text inputs) or patches (for image inputs) during each iteration. This selective updating allows us to explore targeted modifications that prompt the model to either categorize different inputs as the same class or recognize them as distinct. Unlike traditional approaches where modifications are predetermined, this method lets the model itself guide us to understand which data points belong to specific equivalence classes. To interpret embeddings resulted from the exploration process, they must be mapped back into a human-understandable form, such as text or images. The interpretation of an embedding vector depends on the operations performed by the Transformer’s embedding module e_T . If e_T consists only of invertible operations, it is feasible to construct a layer that performs the inverse operation relative to e_T . The output can then be visualized and directly interpreted by humans, allowing for a comparison with the original input to discern how differences in embeddings reflect differences in their representations (e.g., text, images). If the operations in e_T are non-invertible, a trained decoder is required to reconstruct an interpretable output from each embedding matrix $p_0 \dots p_K$. When using a BERT model, it is feasible to utilize layers that are specialized for the masked language modeling (MLM) task to map input embeddings back to tokens. This approach is effective whether the BERT model in question is specifically designed for MLM or for sentence classification. In the case of sentence classification models, it is necessary to select a corresponding MLM BERT model that shares the same internal architecture, including the number of layers and embedding size.

Algorithm 5 depicts the process of interpreting Algorithm 4 outputs for both ViT and BERT experiments. After initializing the decoder according to the model type, the embeddings $p_0 \dots p_K$ need to be constrained to a feasible region. This region is defined by the distribution of embeddings derived from the original input instances. Next, the embeddings are decoded, and the selected segments for exploration are extracted. These segments are then used to replace the corresponding parts of the original input instance. Figure 3 depicts an example outcome of Algorithm 5 applied on a ViT

Algorithm 5 Interpretation for Exploration results for ViT and BERT models.

- 1: **Inputs:**
- 2: Transformer model T with: Tokenizer t_T , Embedding layer e_T , Intermediate layers l_T
- 3: Modified embeddings $p_0 \dots p_K$ resulted from Algorithm 4 applied on an input x
- 4: $P = \{p | p \in x^t\}$ indices of updated segments
- 5: **If** T is ViT:
- 6: Initialize decoder d with weights from e_T .
- 7: **If** T is BERT:
- 8: Initialize decoder with intermediate and final layers of a BERT for MLM task.
- 9: Compute embeddings distributions for original input data
- 10: Use the original embeddings distributions to cap $p_0 \dots p_K$
- 11: Decode modified embeddings $p_0 \dots p_K$ using d to generate the corresponding images/sentences $X' = x'_0 \dots x'_K$.
- 12: **For each** $x' \in X'$: replace segments relative to indices P in x with those in x' .
- 13: **Outputs:**
- 14: Modified input images/sentences, one for each SiMEC/SiMExp iteration.

exploration experiment. Given that the interpretation process includes both a capping step and a

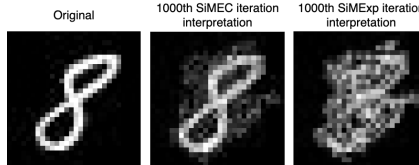


Figure 3: Example of SiMEC and SiMExp output interpretation for ViT digit classification. Left: Original MNIST image of an “8”. Center: Interpretation of a p_{1000} from a SiMEC experiment, where p_{1000} is predicted as “8”. Right: Interpretation of a p_{1000} from a SiMExp experiment, where p_{1000} is predicted as “4”. All patches are subject to SiMEC and SiMExp updates.

decoding step (lines 10 and 11 of Algorithm 5), it’s important to note that there isn’t a direct 1:1 correspondence between each iteration’s update and the interpretation outcomes. Our primary focus is on exploring the input embedding space, rather than the input image or input sentence spaces.

For further investigation, we provide a detailed discussion on considering interpretation outputs as alternative prompts in Section 4.

4 Experiments

Experiments are conducted on textual and visual data. We aim to perform a preliminary investigation of 3 features of our approach: (i) how the class probability changes on the decoded output of SiMEC/SiMExp, (ii) what is the trade-off between the quantity and the quality of the output, and (iii) how our method can be used to extract feature importance-based explanations.

In the textual case, we experiment with hate speech classification datasets: we use HateXplain² [13], which provides a ground truth for feature importance, plus a sample of 100 hate speech sentences generated by prompting ChatGPT³, which serve purposes (i) and (ii). In the visual case, we perform experiments on MNIST [12] dataset.

Using interpretation outputs as alternative prompts An interesting investigation is to determine if our interpretation algorithm (Algorithm 5) can generate alternative prompts that stay in the same equivalence class as the original input data or move to a different one, based on SiMEC and SiMExp explorations. We test how the probability assigned to the original equivalence class by the Transformer model changes as the SiMEC and SiMExp algorithms explore the input embedding manifold.

For BERT experiments we generate prompts to inspect the probability distribution over the vocabulary for tokens updated by Algorithms 1 and 2. We decode the updated $p_0 \dots p_K$ using Algorithm 5, focusing on tokens updated through the iterations. For each of these decoded tokens, we extract the top-5 scores to obtain 5 alternative tokens to replace the original ones, creating 5 alternate prompts. We then extract the prediction $i^* = \arg \max_i y_i$ for the original sentence, which represents the output whose equivalence class we aim to explore. Finally, we classify the new prompts, obtaining the corresponding predictions $Y = y^{(0)} \dots y^{(K)}$, where each $y^{(k)} \in \mathbb{R}^N$, N being the number of prediction classes. We visualize the prediction trend for the i^* th value in every $y^{(0)} \dots y^{(K)}$ categorizing the images into two subsets: those that lead to a change in prediction $Y_c = \{y^{(k)} \in Y \mid \arg \max_i y_i^{(k)} \neq i^*\}$ and those that don't $Y_s = \{y_i \in Y \mid \arg \max_i y_i^{(k)} = i^*\}$.

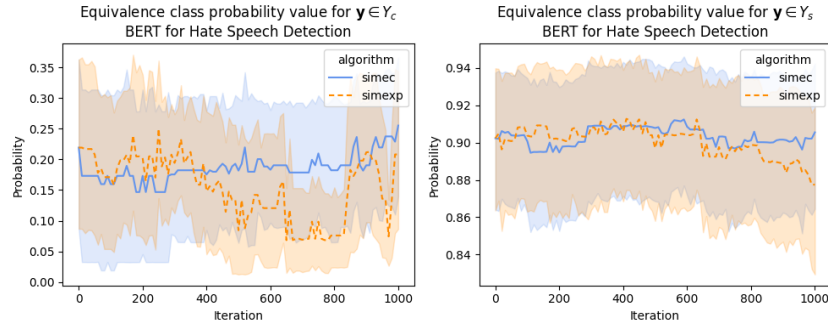


Figure 4: Analysis involving results SiMEC and SiMExp applied to BERT for hate speech detection. Left: Prediction values for i^* for each $y \in Y_c$. Right: Prediction values for $y \in Y_s$.

Sentence classification experiments⁴ involved 1000 iterations from both SiMEC and SiMExp, applied to a subset of 8 sentences from the ChatGPT hate speech dataset. The plot on the left side of Figure 4 illustrates that, as the original embeddings are increasingly modified, SiMExp tends to produce alternatives with lower prediction values for i^* compared to SiMEC. Thus, even if predictions change in SiMEC experiments, the equivalence class prediction value remains approximately constant and higher than in SiMExp. Considering the plot on the right side of Figure 4, SiMExp identifies prompts

²MIT License

³Used prompts are included in the Supplementary Materials.

⁴Model used: huggingface.co/ctoraman/hate-speech-bert

that lower the prediction value for i^* . ViT and MLM experiments are detailed in the Supplementary Materials.

Input space exploration We measure the time required to explore the input space of a ViT with the SiMEC algorithm and compare it with a perturbation-based method. The perturbation-based method mimics a trial-and-error approach as it takes an input image and, at each iteration, perturbs it by a semi-random vector $\mathbf{v}_{t+1} = a_t \mathbf{v}_t + \eta \epsilon$, where $a_t = 1$ if $y_t = y_{t-1}$, $a_t = -1$ otherwise, ϵ is an orthogonal random vector from a standard normal distribution and η is the step length. With the perturbation, we obtain a new image, then check whether the model yields the same label for the new image. The perturbation vector is re-initialized at random from a normal distribution 20% of the times to allow for exploration. We construct this method to have a direct comparison with ours in the absence of a consolidated literature about the task.

We train a ViT model having 4 layers and 4 heads per layer on the MNIST dataset⁵. The SiMEC algorithm is run for 1000 iterations, so that it can generate 1000 examples starting from a single image. In a sample of 100 images, the average time is approximately 339 seconds.⁶ In the same time, the perturbation-based algorithm can produce up to 36000 images. However, we notice that the perturbation-based algorithm ends up producing monochrome (pixel color has zero variance) or totally noisy images, which provide little information about the behavior of the model. Excluding only the images with low color variance (< 0.01), we are left, on average, with 19 images (standard deviation 13.9). SiMEC, in contrast, doesn't present this behavior, as all 1000 images have high enough intensity variance and are thus useful for explainability purposes.

As BERT has many more parameters with respect to our ViT model, processing textual data takes longer. Specifically, in a sample of 16 sentences, the average time needed to run 1000 iterations on a sentence is 7089 seconds, taking into account both MLM and classification experiments.

Feature importance-based explanations We compare our method against Attention Rollout (AR) [1] and the Relevancy method proposed by Chefer et al. [6]. In the textual case, we provide a quantitative evaluation using the HateXplain dataset, which contains 20147 sentences (of which 1924 in the test set) annotated with *normal*, *offensive* and *hate speech* labels as well as the positions of words that support the label decision. We then measure the cosine similarity between the importance assigned by each method to each word in a sentence and the ground truth. Notice that, since the dataset contains multiple annotations, the ground truth y for each word w is obtained as the average of the binary labels assigned by each annotator, and therefore $y(w) \in [0; 1]$. We also normalize all scores in $[0; 1]$ so to have them on the same scale. The average similarity achieved by our method is **0.707** (standard deviation $\sigma = 0.302$), against **0.7** ($\sigma = 0.315$) for Relevancy and **0.583** ($\sigma = 0.318$) for AR. This proves our method to be more effective in finding the most sensitive tokens for classification. We provide an example on image classification in the Supplementary Materials.

5 Related work

Our work relates to embedding space exploration literature, and has at least one collateral applications in the XAI domain, namely producing feature importance-based explanations.

Embedding space exploration. Works dealing with embedding space exploration mostly focus on the study of specific properties of the embedding space of Transformers, especially in NLP. For instance, Cai et al. [5] challenge the idea that the embedding space is inherently anisotropic [10] discovering local isotropy, and find low-dimensional manifold structures in the embedding space of GPT and BERT. Bić et al. [3] argue that the anisotropy of the embedding space derives from embeddings shifting in common directions during training. In the field of CV, Vilas et al. [21] map internal representations of a ViT onto the output class manifold, enabling the early identification of class-related patches and the computation of saliency maps on the input image for each layer and head. Applying Singular Value Decomposition to the Jacobian matrix of a ViT, Salman et al. [17] treat the input space as the union of two subspaces: one in which image embedding doesn't change,

⁵Using Adam optimizer, the model achieved the highest validation accuracy (96.25%) in 20 epochs.

⁶All experiments are based on the current PyTorch implementation of the algorithms and run on a Ubuntu 20.04 machine endowed with one NVIDIA A100 GPU and CUDA 12.4.

and another one for which it changes. Except for the last one, all the aforementioned approaches rely on data samples. By studying the inverse image of the model, instead, we can do away with data samples.

Feature importance-based explanations. Feature importance is a measure of the contribution of each data feature to a model prediction. In the context of Computer Vision and Natural Language Processing, it amounts to giving a weight to pixels (or patches of pixels) in an image and tokens in a piece of text, respectively. In recent years, much research has focused on Transformers in both CV and NLP. Most approaches are based on the attention mechanism of the Transformer architecture. Abnar and Zuidema [1] quantify the overall attention of the output on the input by computing a linear combination of layer attentions (Attention Rollout) or applying a maximum flow algorithm (Attention Flow). To overcome the limitations [4] of attention-based methods, Hao et al. [11] use the concept of *attribution*, which is obtained by multiplying attention matrices by the integrated gradient of the model with respect to them. Chefer et al. [6] propose the Relevancy metric to generalize attribution to bi-modal and encoder-decoder architectures. Other methods are perturbation-based, where perturbations of input data are used to record any change in the output and draw a saliency map on the input. In order to overcome the main issue with such methods, i.e. the generation of outlier inputs, Englebert et al. [9] apply perturbations after the position encoding of the patches. In contrast with these methods, ours does not need arbitrary perturbations of inputs, and considers all parameters of the model, not only the attention query and key matrices.

6 Conclusions

Our exploration of the Transformer architecture through a theoretical framework grounded in Riemannian Geometry led to the application of our two algorithms, SiMEC and SiMExp, for examining equivalence classes in the Transformers’ input space. We demonstrated how the results of these exploration methods can be interpreted in a human-readable form and conducted preliminary investigations into their potential applications. Notably, our methods show promise for ranking feature importance and generating alternative prompts within the same or different equivalence classes.

Future research directions include expanding our experimental results and delving deeper into the potential of our framework for controlled input generation within an equivalence class. This application holds significant promise for enhancing the explainability of Transformer models’ decisions and for addressing issues related to bias and hallucinations.

Acknowledgments and Disclosure of Funding

References

- [1] S. Abnar and W. Zuidema. Quantifying attention flow in transformers. 2020. arXiv:2005.00928.
- [2] A. Benfenati and A. Marta. A singular Riemannian geometry approach to Deep Neural Networks I. Theoretical foundations. *Neural Networks*, 158:331–343, 2023.
- [3] D. Biś, M. Podkorytov, and X. Liu. Too much in common: Shifting of embeddings in transformer language models and its implications. In *Proceedings of the 2021 conference of the North American chapter of the Association for Computational Linguistics: Human Language Technologies*, pages 5117–5130, 2021.
- [4] G. Brunner, Y. Liu, D. Pascual, O. Richter, M. Ciaramita, and R. Wattenhofer. On identifiability in transformers. *International Conference on Learning Representations*, 2019.
- [5] X. Cai, J. Huang, Y. Bian, and K. Church. Isotropy in the contextual embedding space: Clusters and manifolds. In *International conference on learning representations*, 2020.
- [6] H. Chefer, S. Gur, and L. Wolf. Generic attention-model explainability for interpreting bi-modal and encoder-decoder transformers. In *Proceedings of the IEEE/CVF International Conference on Computer Vision*, pages 397–406, 2021.

[7] J. Devlin, M.-W. Chang, K. Lee, and K. Toutanova. BERT: Pre-training of deep bidirectional transformers for language understanding. In J. Burstein, C. Doran, and T. Solorio, editors, *Proceedings of the 2019 Conference of the North American Chapter of the Association for Computational Linguistics: Human Language Technologies, Volume 1 (Long and Short Papers)*, pages 4171–4186, Minneapolis, Minnesota, June 2019. Association for Computational Linguistics. doi: 10.18653/v1/N19-1423. URL <https://aclanthology.org/N19-1423>.

[8] A. Dosovitskiy, L. Beyer, A. Kolesnikov, D. Weissenborn, X. Zhai, T. Unterthiner, M. Dehghani, M. Minderer, G. Heigold, S. Gelly, J. Uszkoreit, and N. Houlsby. An image is worth 16x16 words: Transformers for image recognition at scale, 2021. arXiv:2010.11929.

[9] A. Englebert, S. Stassine, G. Nanfack, S. A. Mahmoudi, X. Siebert, O. Cornu, and C. De Vleeschouwer. Explaining through transformer input sampling. In *Proceedings of the IEEE/CVF International Conference on Computer Vision*, pages 806–815, 2023.

[10] J. Gao, D. He, X. Tan, T. Qin, L. Wang, and T.-Y. Liu. Representation degeneration problem in training natural language generation models. In *International conference on learning representations*, volume abs/1907.12009, 2019. URL <https://api.semanticscholar.org/CorpusID:59317065>.

[11] Y. Hao, L. Dong, F. Wei, and K. Xu. Self-attention attribution: Interpreting information interactions inside transformer. In *Proceedings of the AAAI Conference on Artificial Intelligence*, volume 35, pages 12963–12971, 2021.

[12] Y. Lecun, L. Bottou, Y. Bengio, and P. Haffner. Gradient-based learning applied to document recognition. *Proceedings of the IEEE*, 86(11):2278–2324, 1998. doi: 10.1109/5.726791.

[13] B. Mathew, P. Saha, S. M. Yimam, C. Biemann, P. Goyal, and A. Mukherjee. Hateexplain: A benchmark dataset for explainable hate speech detection. In *Proceedings of the AAAI conference on artificial intelligence*, volume 35, pages 14867–14875, 2021.

[14] N. Papernot, P. McDaniel, S. Jha, M. Fredrikson, Z. B. Celik, and A. Swami. The Limitations of Deep Learning in Adversarial Settings. In *2016 IEEE European Symposium on Security and Privacy (EuroS&P)*, pages 372–387, Mar. 2016. doi: 10.1109/EuroSP.2016.36.

[15] F. Rellich and J. Berkowitz. *Perturbation Theory of Eigenvalue Problems*. New York University. Institute of Mathematical Sciences. Gordon and Breach, 1969. ISBN 9780677006802.

[16] M. T. Ribeiro, S. Singh, and C. Guestrin. "why should i trust you?" explaining the predictions of any classifier. In *Proceedings of the 22nd ACM SIGKDD international conference on knowledge discovery and data mining*, pages 1135–1144, 2016.

[17] S. Salman, M. M. B. Shams, and X. Liu. Intriguing equivalence structures of the embedding space of vision transformers, 2024. arXiv:2401.15568.

[18] M. E. Taylor. *Partial differential equations. I: Basic theory*, volume 115 of *Appl. Math. Sci.* Cham: Springer, 3rd corrected and expanded edition edition, 2023. ISBN 978-3-031-33858-8; 978-3-031-33861-8; 978-3-031-33859-5. doi: 10.1007/978-3-031-33859-5.

[19] C. Toraman, F. Şahinuç, and E. H. Yilmaz. Large-scale hate speech detection with cross-domain transfer. In *Proceedings of the Language Resources and Evaluation Conference*, pages 2215–2225, Marseille, France, June 2022. European Language Resources Association. URL <https://aclanthology.org/2022.lrec-1.238>.

[20] L. N. Trefethen and D. I. Bau. *Numerical linear algebra. Twenty-fifth anniversary edition*, volume 181 of *Other Titles Appl. Math.* Philadelphia, PA: Society for Industrial and Applied Mathematics (SIAM), 2022. ISBN 978-1-61197-715-8.

[21] M. G. Vilas, T. Schaumlöffel, and G. Roig. Analyzing vision transformers for image classification in class embedding space. *Advances in Neural Information Processing Systems*, 36, 2024.

[22] M. Wu, H. Wu, and C. Barrett. Verix: Towards verified explainability of deep neural networks. *Advances in neural information processing systems*, 36, 2024.

Supplementary material

Anonymous Author(s)

Affiliation
Address
email

1 **1 Definitions**

2 First we recall our geometric definitions of neural network and layer.

3 **Definition 1** (Neural Network). *A neural network is a sequence of \mathcal{C}^1 maps Λ_i between manifolds of
4 the form:*

$$M_0 \xrightarrow{\Lambda_1} M_1 \xrightarrow{\Lambda_2} M_2 \xrightarrow{\Lambda_4} \dots \xrightarrow{\Lambda_{n-1}} M_{n-1} \xrightarrow{\Lambda_n} M_n \quad (1)$$

5 We call M_0 the input manifold and M_n the output manifold. All the other manifolds of the sequence
6 are called representation manifolds. The maps Λ_i are the layers of the neural network. We denote
7 with $\mathcal{N}_{(i)} = \Lambda_n \circ \dots \circ \Lambda_i : M_i \rightarrow M_n$ the mapping from the i -th representation layer to the output
8 layer.

9 **Definition 2** (Smooth layer). *A map $\Lambda_i : M_{i-1} \rightarrow M_i$ is called a smooth layer if it is the restriction
10 to M_{i-1} of a function $\bar{\Lambda}^{(i)}(x) : \mathbb{R}^{d_{i-1}} \rightarrow \mathbb{R}^{d_i}$ of the form*

$$\bar{\Lambda}_{\alpha}^{(i)}(x) = F_{\alpha}^{(i)} \left(\sum_{\beta} A_{\alpha\beta}^{(i)} x_{\beta} + b_{\alpha}^{(i)} \right) \quad (2)$$

11 for $i = 1, \dots, n$, $x \in \mathbb{R}^{d_i}$, $b^{(i)} \in \mathbb{R}^{d_i}$ and $A^{(i)} \in \mathbb{R}^{d_i \times d_{i-1}}$, with $F^{(i)} : \mathbb{R}^{d_i} \rightarrow \mathbb{R}^{d_i}$ a diffeomor-
12 phism.

13 We also need some standard definitions in differential geometry [4].

14 **Definition 3** (Submersion). *Let $f : M \rightarrow N$ be a smooth map between manifolds. Then f is a
15 submersion if, in any chart, the Jacobian J_f has rank $\dim(N)$.*

16 **Definition 4** (Embedding). *Let $f : M \rightarrow N$ be a smooth map between manifolds. f is an embedding
17 if its differential is everywhere injective and if it is an homeomorphism with its image. In other words,
18 f is a diffeomorphism with its image.*

19 **Definition 5** (Distribution). *A distribution \mathcal{D} of dimension k over a m -dimensional manifold M is a
20 collection of k smooth vector fields v_1, \dots, v_k such that $(v_1)_p, \dots, (v_k)_p$ form a basis of a vector
21 subspace of dimension k in $T_p M$ for every $p \in M$.*

22 **Definition 6** (Integrable distribution). *A distribution \mathcal{D} of dimension k is an integrable distribution
23 if there exist a manifold M of dimension $m \geq k$ such that the collection of k smooth vector fields
24 v_1, \dots, v_k are generating a vector space of dimension k over $T_p M$ for all $p \in M$.*

25 **Definition 7** (Trivial fiber bundle). *A trivial fiber bundle is a structure (E, B, π, F) , where E, B and
26 F are topological spaces with $E = B \times F$ and the map $\pi : E \rightarrow B$ is the projection of $B \times F$ on
27 B . The space F is called typical fiber. In the case F is a vector space, then (E, B, π, F) is called a
28 trivial vector bundle.*

29 **Definition 8** (Vertical and horizontal spaces). *Let (E, M, π, F) be a vector bundle over a manifold
30 M . Then the vertical space $\mathcal{V}_p E$ at $p \in E$ is the vector space $\mathcal{V}_p E = \text{Ker}(d_p \pi) \subset T_p E$. The
31 horizontal space $\mathcal{H}_p E$ is a choice of a subspace of $T_p E$ such that $T_p E = \mathcal{V}_p E \oplus \mathcal{H}_p E$. The spaces
32 $\mathcal{V} E := \bigsqcup_{p \in E} \mathcal{V}_p E$ and $\mathcal{H} E := \bigsqcup_{p \in E} \mathcal{H}_p E$ are two bundles called vertical and horizontal bundles
33 respectively.*

34 **2 Hypotheses**

35 In the following lemmas and propositions we always assume the following hypotheses to hold true.

36 **Assumption 1.** *The manifolds M_i are open and path-connected sets of dimension $\dim M_i = d_i$.*

37 **Assumption 2.** *The sequence of maps (1) satisfies the following properties:*

38 1) *If $\dim(M_{i-1}) \leq \dim(M_i)$ the map $\Lambda_i : M_{i-1} \rightarrow M_i$ is a smooth embedding.*

39 2) *If $\dim(M_{i-1}) > \dim(M_i)$ the map $\Lambda_i : M_{i-1} \rightarrow M_i$ is a smooth submersion.*

40 **Assumption 3.** *The manifold M_n is equipped with the structure of Riemannian manifold, with metric
41 $g^{(n)}$.*

42 **Assumption 4.** *We assume that the manifolds M_i are diffeomorphic to \mathbb{R}^{d_i} for some $d_1, \dots, d_n \in \mathbb{N}$.*

43 **Assumption 5.** *The matrices of weights in the maps Λ_i , $i = 1, \dots, n$, as per in Definition 2 are of
44 full rank.*

45 **3 Proof of the propositions**

46 **Proposition 1.** *Let $\gamma : [0, 1] \rightarrow M_i$ be a piecewise \mathcal{C}^1 curve. Let $k \in \{i, i+1, \dots, n\}$ and consider
47 the curve $\gamma_k = \Lambda_k \circ \dots \circ \Lambda_i \circ \gamma$ on M_k . Then $Pl_i(\gamma) = Pl_k(\gamma_k)$*

48 *Proof.* It is enough to notice that $\gamma_k : (0, 1) \rightarrow M_k$ is still a piecewise \mathcal{C}^1 curve and that

$$\begin{aligned} Pl_k(\gamma_k) &= \int_0^1 \sqrt{g_{\gamma_k(s)}^{(k)}(\dot{\gamma}_k(s), \dot{\gamma}_k(s))} ds \\ &= \int_0^1 \sqrt{((\Lambda_k \circ \dots \circ \Lambda_i)^* g^{(k)})_{\gamma(s)}(\dot{\gamma}(s), \dot{\gamma}(s))} ds \\ &= Pl_i(\gamma) \end{aligned}$$

49 where $(\Lambda_k \circ \dots \circ \Lambda_i)^* g^{(k)}$ is the pullback of $g^{(k)}$ via $\Lambda_k \circ \dots \circ \Lambda_i$. \square

50 **Corollary 1.** *Let $\gamma : [0, 1] \rightarrow M_i$ be a piecewise \mathcal{C}^1 curve. Consider the curve $\Gamma = \mathcal{N}_i \circ \gamma$ on
51 $\mathcal{N}(M_0) \subseteq M_n$. Then $Pl_i(\gamma) = Pl_n(\Gamma)$, with L_n the length of a curve defined using the Riemannian
52 metric $g^{(n)}$.*

53 *Proof.* The thesis immediately follows from Proposition 1 setting $k = n$. \square

54 **Lemma 1.** *M_i / \sim_i is an open, path-connected, Hausdorff, second-countable set.*

55 *Proof.* An elementary property of quotient maps yields that M_i / \sim_i is still a path-connected space
56 and by [3, Corollary 3.17] we also know that π_i is an open map, therefore the quotient set M_i / \sim_i is
57 open. Since pseudometric spaces are completely regular [3, Section 7], we conclude that M_i / \sim_i
58 is Tychonoff and therefore it is in particular T_2 . At last we note that, since π_i is an open quotient,
59 M_i / \sim_i is also second-countable. \square

60 **Proposition 2.** *If two points $p, q \in M_i$ are in the same class of equivalence, then $\mathcal{N}_i(p) = \mathcal{N}_i(q)$.*

61 *Proof.* Let $p, q \in M_i$ two points in the same class of equivalence $[p]$. Then, since M_i is path
62 connected by hypothesis, there is a piecewise \mathcal{C}^1 null curve $\gamma : [0, 1] \rightarrow M_0$ connecting q and p , with
63 $Pl_i(\gamma) = 0$. Consider now the curve $\Gamma = \mathcal{N}_i \circ \gamma$ on M_n . By Corollary 1 we conclude that also
64 $Pl_n(\Gamma) = 0$ and being $g^{(n)}$ a Riemannian metric we have that $\mathcal{N}_i(p) = \mathcal{N}_i(q)$. \square

65 **Proposition 3.** *Let $x, y \in M_i$, then $x \sim_i y$ if and only if $x \sim_{\mathcal{N}_i} y$.*

66 *Proof.* If $x \sim_i y$, then there is a piecewise \mathcal{C}^1 null curve γ with $\gamma(0) = x$ and $\gamma(1) = y$ and we have
67 that $Pl_i(\gamma) = Pl_n(\mathcal{N}_i \circ \gamma) = 0$. Since $g^{(n)}$ is a non-degenerate Riemannian metric, $Pl_n(\mathcal{N}_i \circ \gamma) = 0$
68 entails that the tangent vector to $\mathcal{N}_i \circ \gamma(s)$ is the zero vector for every $s \in (0, 1)$ and therefore $\mathcal{N}_i \circ \gamma$
69 is the constant curve $\mathcal{N}_i \circ \gamma(s) = \mathcal{N}_i(x)$. This proves $x \sim_i y \Rightarrow x \sim_{\mathcal{N}_i} y$. Let us now assume

70 that $x \sim_{\mathcal{N}_i} y$. By definition we know that there is a piecewise \mathcal{C}^1 curve $\gamma : [0, 1] \rightarrow M_i$ such that
 71 $\gamma(0) = x, \gamma(1) = y$ and $\mathcal{N}_i \circ \gamma(s) = \mathcal{N}_i(x) \forall s \in [0, 1]$. It remains to prove that γ is a null curve.
 72 This follows from the fact that, being $\mathcal{N}_i \circ \gamma$ a constant curve, then $Pl_i(\gamma) = l(\mathcal{N} \circ \gamma) = 0$. \square

73 **Corollary 2.** *Under the hypothesis of Proposition 3, one has that $M_i/\sim_i = M_i/\sim_{\mathcal{N}_{i+1}}$. Moreover,*
 74 *if two points $p, q \in M_i$ are connected by a \mathcal{C}^1 curve $\gamma : [0, 1] \rightarrow M_i$ satisfying $\mathcal{N}_i(p) = \mathcal{N}_i \circ \gamma(s)$*
 75 *for every $s \in [0, 1]$, then they lie in the same class of equivalence.*

76 *Proof.* The statement follows immediately from Propositions 2 and 3 making use of the definitions
 77 of the quotients \sim_i and $\sim_{\mathcal{N}_{i+1}}$. \square

78 **Theorem 1** (Godement's criterion, [2, 1]). *Let X be a smooth manifold and $R \subset X \times X$ be an*
 79 *equivalence relation. The quotient X/R is a smooth manifold if and only if*

80 1) *R is a submanifold of $X \times X$*
 81 2) *The projection map on the second component $pr_2 : R \subset X \times X \rightarrow X$ is a submersion.*

82 Now we can prove that M_i/\sim_i is a smooth manifold.

83 **Proposition 4.** $\frac{M_i}{\sim_i}$ *is a smooth manifold of dimension $\dim(\mathcal{N}(M_0))$.*

84 *Proof.* We prove that the quotient M_i/\sim_i is a smooth manifold using Godement's criterion (Theorem 1). The graph \mathcal{G}_{i+1} of $\sim_{\mathcal{N}_i}$ is the union of $C_p \times C_p$, with C_p a connected component of $\mathcal{N}_i^{-1}(p)$,
 85 with $p \in \mathcal{N}_i(M_{i-1}) \subseteq M_n$ and therefore \mathcal{G}_{i+1} is a submanifold of $M_i \times M_i$. Furthermore, the
 86 restriction of the projection pr_2 to R is the restriction of the identity map to C_p for some $p \in M_i$,
 87 which is a diffeomorphism with its image and therefore a submersion. The statement about the
 88 dimension follows from the proof of 2) \Rightarrow 1) of Theorem 1, see [2, Lemma 9.4], taking in account
 89 that $T_p N_i = \dim(\text{Ker}(g^{(i)}))$ is constant. \square

91 This proposition, along with [2, Lemma 9.4 and Lemma 9.9], yields that the classes of equivalence
 92 $[p]$ are the leaves of a simple foliation of M_i and that π_i is a smooth submersion.

93 **Proposition 5.** $\pi_i : M_i \rightarrow M_i/\sim_i$ *is a smooth fiber bundle, with $\text{Ker}(d\pi_i) = \mathcal{V}M_i$, which is*
 94 *therefore an integrable distribution. Every class of equivalence $[p]$ is a path-connected submanifold*
 95 *of M_i and coincide with the fiber of the bundle over p .*

96 *Proof.* The first part of the statement follows applying Proposition 4 together with [2, Lemma 9.4 and
 97 Lemma 9.9]. The second part of the statement is then a consequence of the definitions of equivalence
 98 class and vertical bundle. \square

99 4 ChatGPT prompts

100 In order to generate a small dataset of 100 sentences for hate speech detection, we prompt ChatGPT
 101 (3.5 version) with several requests. The first one is: *can you generate 100 sentences with [CLS] and*
 102 *[MASK] tokens as input for BERT? Do not enumerate them while printing them, I want to do a copy*
 103 *paste directly in a txt file.*

104 Then: *can you do the same but generating sentences for training a BERT model for hate speech*
 105 *detection?*

106 And finally: *can you do the same but without the [MASK] token and with some of them being offensive*
 107 *(37%), other hate speech (39%) and others neutral (24%)? Still add the [CLS] token.*

108 This yields the dataset we used for exploration of BERT input embedding space.

109 **5 Using interpretation outputs as alternative prompts (cont.)**

110 ViT experiments were conducted using 1000 iteration outcomes from both SiMEC and SiMExp,
 111 applied to a subset of the MNIST dataset containing 14 images of the digit “4”. BERT for MLM
 112 experiments involved 1000 iterations from both SiMEC and SiMExp, applied to a subset of 8
 113 sentences from the “fill in the mask” dataset (see Section 4 for more details).

114 For ViT experiments, we first extract the original predicted class $i^* = \arg \max_i y_i$, which represents
 115 the output whose equivalence class we aim to explore. Then, we run the interpretation algorithm
 116 for each $p_0 \dots p_K$ to obtain K interpretations in the form of images. Finally, we classify the new
 117 images, obtaining the corresponding predictions $Y = \mathbf{y}^{(0)} \dots \mathbf{y}^{(K)}$, where each $\mathbf{y}^{(k)} \in \mathbb{R}^N$, N
 118 being the number of prediction classes (e.g., $N = 10$ in MNIST). We visualize the prediction
 119 trend for the i^* th value in every $\mathbf{y}^{(0)} \dots \mathbf{y}^{(K)}$ categorizing the images into two subsets: those
 120 that lead to a change in prediction $Y_c = \{\mathbf{y}^{(k)} \in Y \mid \arg \max_i y_i^{(k)} \neq i^*\}$ and those that don’t
 121 $Y_s = \{\mathbf{y}_i \in Y \mid \arg \max_i y_i^{(k)} = i^*\}$.

122 Considering BERT for MLM experiments, we proceed as illustrated in the main text.

123 Figure 1 illustrates a scenario similar to the one described in the main text. Specifically, it shows SiM-
 124 Exp’s tendency to identify modifications that lower the prediction value for the original equivalence
 125 class, i^* .

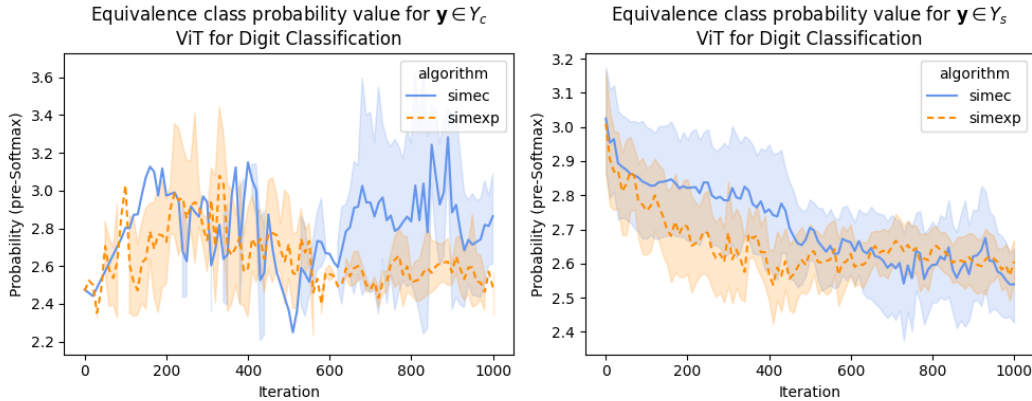


Figure 1: Results of ViT experiments involving 1000 iterations from both SiMEC and SiMExp, applied to subsets of MNIST dataset, each containing 14 sentences. The left plot shows prediction values for i^* for each $\mathbf{y} \in Y_c$, whereas the right plot depicts prediction values for $\mathbf{y} \in Y_s$. In general, both plots show a similar trend where SiMExp generally identifies alternative prompts that lower the prediction value for i^* .

126 Results for experiments using BERT for MLM are depicted in Figure 2. The plot on the left side
 127 exhibits the expected behavior. However, when selecting alternative tokens that lead to the same
 128 equivalence class, SiMExp seems unable to lower the prediction value of i^* . While our primary
 129 concern is validating the expected behavior when the prediction class changes (left plot), a deeper
 130 investigation into using interpretation outputs as prompts will be crucial in future work.

131 **6 Example of feature importance in image classification**

132 As, to the best of our knowledge, we are not aware of any explainable version of the MNIST dataset,
 133 we show the results of the same methods applied to ViT in an example, reported in Figure 3. This
 134 example is in line with the results obtained on the sample of 100 images from the MNIST dataset and
 135 shows that our method gives higher importance to pixels that are contained in the actual shape of the
 136 digit or that would form another digit if white (in the case of 6, these are the upper right ones, which
 137 would transform 6 into 8). Though on different scales, the number of pixels assigned high importance
 138 by our approach is larger than in the AR approach and lower with respect to the Relevancy approach.

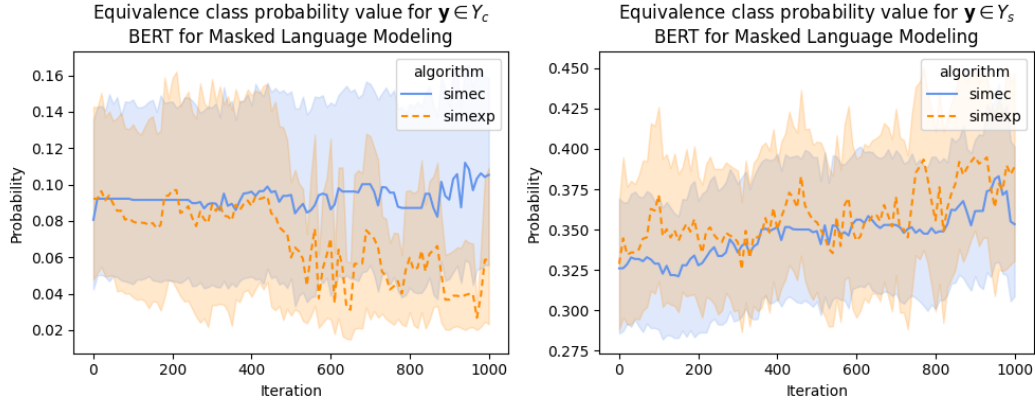


Figure 2: Results of BERT experiments involving 1000 iterations from both SiMEC and SiMExp, applied to subsets of a “fill in the mask” dataset, each containing 8 sentences. The left plot shows prediction values for i^* for each $y \in Y_c$, whereas the right plot depicts prediction values for $y \in Y_s$. Here, the expected behavior can be noted on the left side, where SiMExp tries to predict tokens which in turn lower the probability of the equivalence class prediction i^* . However, the same cannot be said for the plot on the right, where SiMExp is unable to find tokens leading to lower probabilities for i^* .

139 This contributes to give a precise (contrary to AR) and noiseless (contrary to the Relevancy method)
 140 explanation.

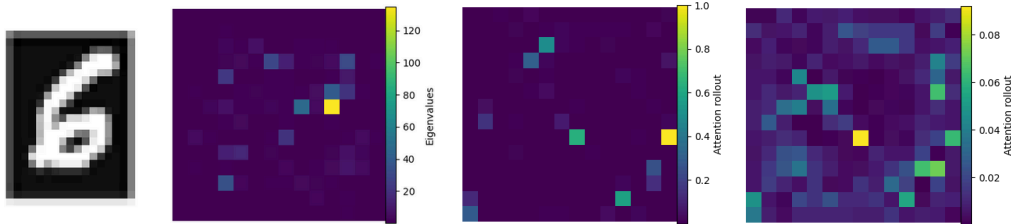


Figure 3: Example of feature importance with our method (left), AR (center) and the Relevancy method (right) on a sample image from the MNIST dataset.

141 References

142 [1] N. Bourbaki. *Variétés différentielles et analytiques: Fascicule de résultats*. Springer-Verlag
 143 Berlin Heidelberg, 1967.

144 [2] R. Fernadnes. Lectures on differential geometry, 2024. To be published by World Scientific,
 145 <https://www.math.tecnico.ulisboa.pt/mabreu/GD/RLF-notes.pdf>.

146 [3] T. Pirttimäki. A survey of Kolmogorov quotients, 2019. arXiv:1905.01157 [math.GN].

147 [4] L. W. Tu. *An Introduction to Manifolds*. Springer-Verlag New York, 2 edition, 2011. doi:
 148 10.1007/978-1-4419-7400-6.